Advanced Quadrotor Takeoff Control Based on Incremental Nonlinear Dynamic Inversion and Integral Extended State Observer

Han Du, Zhiqiang Pu, Jianqiang Yi, Hanbo Qian

***Abstract*—This paper presents an advanced control scheme for quadrotor taking off process. Firstly a high-fidelity model is established, with Coriolis force, gyro effect, and ground effect taken into account. Then the quadrotor control system is decoupled into three control loops, which are position loop, angle loop, and inner loop. Dynamic inversion (DI) is applied to design control laws for both the position and the angle loops. Incremental nonlinear dynamic inverse (INDI) control law is furtherly developed to cope with non-affine form of the inner loop. To realize disturbance rejection and the measurement noise attenuation, integral extended state observer (IESO) is combined in this control scheme. Besides, arranged transient process technique (ATP) is utilized in the control scheme to smooth huge-jump desired input and connect different loops with feasible transient process. Finally, through series of simulations the effectiveness of the control scheme, as well as robustness against external disturbances and measurement noise are validated.**

I. Introduction

A growing interest in quadrotors has been attracted among research communities for the highly rising utilization for both military and civilian purposes. What attract researchers is not only the merits shared with traditional helicopters, but its exclusive characteristics, such as vertically takeoff and land (VTOL), stable hovering, symmetry, and Omni-directional move [1].

With four input and six degrees of freedom, quadrotor is an under-actuated, high-order, highly coupled nonlinear system. Apart from the aerodynamic properties of quadrotor, the Coriolis force, propeller gyro effect, and the ground effect [2] are also unneglectable when modeling for quadrotor during the takeoff process. When it comes to the trajectory and attitude control of quadrotor, the complexity in accurate modeling, inner uncertainties, together with sensitiveness to external disturbance and measurement noise contribute to its complication. Many classical controllers have been developed based on cascaded PID [3], LQR [4], sliding mode [5], back-stepping [6], dynamic inversion (DI) [7], and neutral network [8]. However, the controllers based on PID, LQR, and back-stepping are easily influenced by external disturbances. Sliding mode control is comparatively robust, while its use in quadrotor is restricted owing to the chattering phenomena. DI generally requires complete and accurate model information. Besides, the nonlinear system handled by DI should have the affine form. The incremental nonlinear dynamic inversion (INDI) aims to overcome the drawback and cope with non-affine form system [9]. INDI makes full use of the measurement and contributes to the robustness of system as a result. Ewoud [9] proposed an adaptive INDI controller for the attitude control of micro air vehicle (MAV). The experiments showed high performance and effective disturbance rejection.

The incorporation of state observer makes up for the quadrotor performance in robustness by estimating the disturbances and compensating to the controller. In [10] a high-order sliding mode observer is proposed to estimate the wind disturbance for quadrotor. Active disturbance rejection control (ADRC) proposed by Han [11] provides another better key to disturbance rejection. The centerpiece of ADRC is taking all internal uncertainties and external disturbances considered together, treating it as an extended state to be directly estimated with extended state observer (ESO). ESO shows high estimation efficiency. The integral ESO (IESO) [12] improves the ESO in attenuation of measurement noise.

This paper presents an advanced control scheme for the robust attitude and trajectory tracking control during quadrotor takeoff process. The creativities of the control scheme are expressed mainly in four parts. 1) High-fidelity model including Coriolis force, propeller gyro effect, and ground effect. 2) Three-loop decoupled and fully-actuated scheme based on DI and INDI control laws. 3) IESO applied for disturbance estimation. 4) ATP applied for reference input smoothing. The paper is organized as follows. Dynamic model is given in Section II. The three-loop control scheme is proposed in Section III. Section IV contains the design of IESO and ATP. Simulations are conducted in Section V to validate the effectiveness of the control scheme and the robustness against external disturbance. Finally, the conclusion is given in Section VI.

II. Dynamic Model

A. Quadrotor dynamic model

The quadrotor mainly consists of a cross-shaped rigid frame, with 4 rotors located in ends respectively, whose velocity is $w_i (i = 1,2,3,4)$. The distance between each rotor and the center of gravity is l .The front and rear rotors rotate clockwise, while the other two rotate count-clockwise.

The earth frame E and body frame B are established as [1] to describe quadrotor kinematic model.

*Resrach supported by Foundations under grant #61273149, #61421004, and #B1320133020.

Han Du is with University of Chinese Academy of Sciences and Institute of Automation, Chinese Academy of Science, Beijing, 100190 China, (e-mail: duhan2014@ia.ac.cn).

Zhiqiang Pu is with Institute of Automation, Chinese Academy of Science, Beijing, 100190 China, (corresponding author to provide phone: 86-010-82544639; e-mail: zhiqiang.pu@ia.ac.cn).

Jianqiang Yi is with Institute of Automation, Chinese Academy of Science, Beijing, 100190 China, (e-mail: jianqiang.yi@ia.ac.cn).

Hanbo Qian is with The Center of Coordination & Support of SASTIND, Beijing, 100081 China, (e-mail: hanbo.qian@ia.ac.cn).

978-1-4673-8318-9/16/$31.00©2016 IEEE

$$\dot{\mathbf{X}} = R(\boldsymbol{\xi})\mathbf{V}$$
$$\dot{\boldsymbol{\xi}} = M(\boldsymbol{\xi})\boldsymbol{\Omega} \tag{1}$$

The translational position of the quadrotor is denoted as $\mathbf{X} = (x, y, z)^T$. The roll, pitch and yaw angle are denoted as $\boldsymbol{\xi} = (\phi, \theta, \psi)^T$ respectively. The translational velocity of the quadrotor is denoted as $\mathbf{V} = (u, v, w)^T$. The angular rate vector is $\boldsymbol{\Omega} = (p, q, r)^T$. The rotate matrix from B to E is expressed as

$$R(\boldsymbol{\xi}) = \begin{bmatrix} \mathrm{c}\theta\mathrm{c}\psi & \mathrm{c}\psi\mathrm{s}\theta\mathrm{s}\phi - \mathrm{c}\phi\mathrm{s}\psi & \mathrm{c}\phi\mathrm{c}\psi\mathrm{s}\theta + \mathrm{s}\phi\mathrm{s}\psi \\ \mathrm{c}\theta\mathrm{s}\psi & \mathrm{s}\theta\mathrm{s}\phi\mathrm{s}\psi + \mathrm{c}\phi\mathrm{c}\psi & \mathrm{c}\phi\mathrm{s}\theta\mathrm{s}\psi - \mathrm{c}\psi\mathrm{s}\phi \\ -\mathrm{s}\theta & \mathrm{c}\theta\mathrm{s}\phi & \mathrm{c}\theta\mathrm{c}\phi \end{bmatrix} \tag{2}$$

where c and s are short for the cosine and sine functions.

The derivative form of angle model can be formulated as

$$\begin{bmatrix} \dot{\phi} \\ \dot{\theta} \\ \dot{\psi} \end{bmatrix} = \begin{bmatrix} 0 & \sin\phi\sec\theta & \cos\phi\sec\theta \\ 0 & \cos\phi & -\sin\phi \\ 1 & \sin\phi\tan\theta & \cos\phi\tan\theta \end{bmatrix} \begin{bmatrix} p \\ q \\ r \end{bmatrix} \tag{3}$$

The dynamic model can be formulated according to the Newton-Euler function

$$\left.\begin{aligned} \sum F &= \mathbf{1}_{\mathbf{v}} \frac{\delta \mathbf{V}}{\delta t} + \boldsymbol{\Omega} \times \mathbf{V} \\ \sum M &= J\dot{\boldsymbol{\Omega}} + \boldsymbol{\Omega} \times J\boldsymbol{\Omega} \end{aligned}\right\|, J = \begin{bmatrix} I_x & 0 & 0 \\ 0 & I_y & 0 \\ 0 & 0 & I_z \end{bmatrix} \tag{4}$$

Here J is the inertia matrix of the quadrotor. $I_x \sim I_z$ are the inertia components of three directions. $\mathbf{1}_{\mathbf{v}}$ is the unit vector in direction of $\mathbf{V}$. Denote drag and external disturbance as F_a and $F_{disturb}$. $\mathbf{e_u}$ and $\mathbf{e_z}$ are the component of lift force and the gravity in body frame respectively.

$$\begin{aligned} &\sum F = -mg\mathbf{e_z} + U\mathbf{e_u} - F_a + F_{disturb} \\ &\mathbf{e_u} = (0,0,1)^T, \mathbf{e_z} = (-\sin\theta, \sin\phi\cos\theta, \cos\phi\cos\theta)^T \end{aligned} \tag{5}$$

Denote lift force as $U = k_T \mathbf{w}^T \mathbf{w}$, where k_T is the propeller lift coefficient. Combining (1), (4), (5), the translation model can be given as follows

$$\begin{aligned} \begin{bmatrix} \ddot{x} \\ \ddot{y} \\ \ddot{z} \end{bmatrix} &= \frac{1}{m} \begin{bmatrix} (\cos\psi\sin\theta\cos\phi + \sin\psi\sin\phi)U \\ (\sin\psi\sin\theta\cos\phi - \cos\psi\sin\phi)U \\ \cos\theta\cos\phi U - mg \end{bmatrix} \\ &+ \underbrace{R(\boldsymbol{\xi}) \begin{bmatrix} qw - rv \\ ru - pw \\ pv - qu \end{bmatrix}}_{f_{col}} + \underbrace{R(\boldsymbol{\xi}) \begin{bmatrix} -k_{a1}u + \Delta f_x \\ -k_{a2}v + \Delta f_y \\ -k_{a3}w + \Delta f_z \end{bmatrix}}_{Whole\ \Delta f} \end{aligned} \tag{6}$$

in which the second term and the third term are the Coriolis force and total external disturbance respectively.

When it comes to angular dynamic modeling, the total torque of the quadrotor is

$$\sum M = M_d + M_r + M_g \tag{7}$$

where M_d is the disturbance torque. $M_r = (\tau_\phi, \tau_\theta, \tau_\psi)^T$ is the torque generated by the four rotors. M_g is torque generated by propeller gyro effect. Denoting k_d as propeller torque coefficient, J_r as the inertia coefficient of rotor, $\mathbf{w}$ as the velocity vector of the four rotors, we have

$$M_r = G_0 diag(\mathbf{w})\mathbf{w} \quad M_g = G_1\dot{\mathbf{w}} + G_2\mathbf{w} \tag{8}$$

$$G_0 = \begin{bmatrix} 0 & -lk_T & 0 & lk_T \\ lk_T & 0 & -lk_T & 0 \\ k_d & -k_d & k_d & -k_d \end{bmatrix}, G_1 = \begin{bmatrix} 0 & 0 & 0 & 0 \\ 0 & 0 & 0 & 0 \\ J_r & J_r & J_r & J_r \end{bmatrix} \tag{9}$$

$$G_2 = \begin{bmatrix} -J_r q & J_r q & -J_r q & J_r q \\ J_r p & -J_r p & J_r p & -J_r p \\ 0 & 0 & 0 & 0 \end{bmatrix} \tag{10}$$

Combining (4), (8), the angular dynamic model can be formulated as

$$\begin{aligned} \dot{p} &= \frac{I_y - I_z}{I_x} qr - \frac{J_r}{I_x} q\Omega + \frac{1}{I_x}\tau_\phi + \Delta f_p \\ \dot{q} &= \frac{I_z - I_x}{I_y} qr + \frac{J_r}{I_y} p\Omega + \frac{1}{I_y}\tau_\theta + \Delta f_q \\ \dot{r} &= \frac{I_x - I_y}{I_z} qr + \frac{J_r}{I_z}\dot{\Omega} + \frac{1}{I_y}\tau_\psi + \Delta f_r \\ \Omega &= w_1 - w_2 + w_3 - w_4 \end{aligned} \tag{11}$$

where the second terms in first three equations of (11) express the torque generated by the propeller gyro effect. $\Delta f_p \sim \Delta f_r$ are un-modeled angular dynamics and the unknown disturbances. (3), (6), and (11) describe the dynamic model of quadrotor.

B. Ground Effect Model

The ground effect is the phenomena that the apparent thrust of the quadrotor is increased due to the effect that the ground plane has on the downward flow of the rotors, which is firstly researched by Cheeseman [2]. When we try to establish the quadrotor takeoff dynamic model, the ground effect is unneglectable. The ground effect model discussed in [2] was based on a single propeller, which can not attach to the quadrotor. Inspired by the experiment on quadrotor ground effect in [13], the ground effect model can be shown as

$$\begin{aligned} G_{ef}(z) &= \frac{U_{real}}{U_{rotor}} = \begin{cases} \dfrac{1}{1 - \eta(\dfrac{r}{4(z + z_{cg})})^2} & 0.5r < z < 4r \\ 1 & otherwise \end{cases} \\ z_{cg} &= z_r - z_g \end{aligned} \tag{12}$$

where U_{rotor} is the lift force, U_{real} is the whole thrust generated from the four rotors with ground effect influencing. z_r is the altitude of the rotors. z_g is the altitude of the center of gravity. r is the radius of the rotor. η is the coefficient determined by the structure of multiple rotors, for quadrotor $\eta \approx 8$. The

functioning region of the ground effect is $0.5r < z < 4r$ [13]. Update the thrust in (6) with $G_{ef}(z)$

$$U' = k_T \mathbf{w}^T \mathbf{w} / G_{ef}(z) \tag{13}$$

III. Control Scheme Design

In our control scheme, the quadrotor control system is decoupled into three fully actuated control loops according to the time-scale separation principle. The position loop and the angle loop are affine form and controlled by dynamic inversion (DI). The position loop gives the desired angles to the angle loop. Similarly, the angle loop outputs are desired angular rate in inner loop. In the inner loop, the altitude control is combined with the angular rate for the establishment of a fully-actuated subsystem, with the velocity of rotors designed as control input. Furthermore, control law based on incremental nonlinear dynamic inversion (INDI) is developed to cope with non-affine form of the inner loop.

The integral extended state observer (IESO) is one of important part in our control scheme. Both inner uncertainties and external disturbances are observed by IESO. The inner and outer IESO are designed to observe position states and angular states. Furthermore, the arranged transient process (ATP) technique is applied to smooth the huge jump of desired value before the input of the three loops. The three-loop control scheme is depicted in Figure 1.

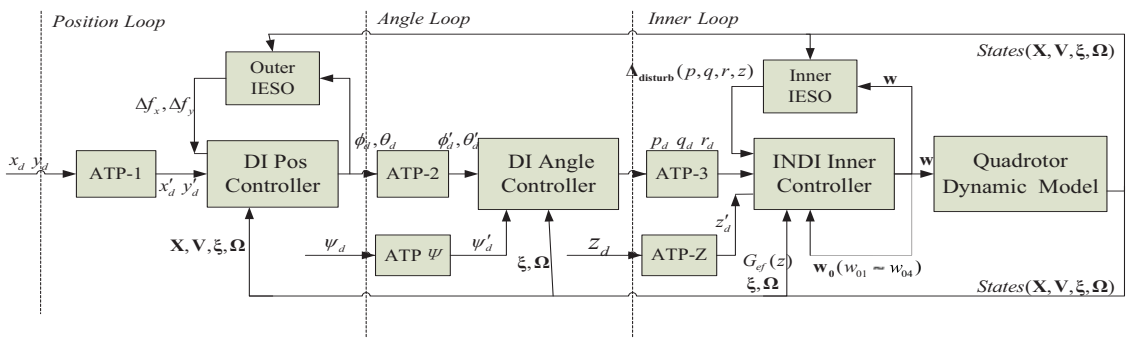

Figure 1. Configuration of three-loop control scheme.

A. DI Controller Design for the Position and Angle Loop

Since the angle loop differential equations in (3) and the position differential equation in (6) are affine-form, dynamic inversion (DI) is applied to design control laws for them.

Denote $R(\xi, i)$ as the column component of $R(\xi)$ in (2). Consider the position loop subsystem model

$$\begin{bmatrix} \ddot{x} \\ \ddot{y} \end{bmatrix} = \frac{U}{m} \begin{bmatrix} (\cos\psi \sin\theta \cos\phi + \sin\psi \sin\phi) \\ (\sin\psi \sin\theta \cos\phi - \cos\psi \sin\phi) \end{bmatrix} + \begin{bmatrix} R(\xi,1) \\ R(\xi,2) \end{bmatrix} \begin{bmatrix} qw - rv \\ ru - pw \\ pv - qu \end{bmatrix} + \begin{bmatrix} \Delta f_x \\ \Delta f_y \end{bmatrix} \tag{14}$$

Denote virtual control input as $\alpha = \sin\phi, \beta = \sin\theta\cos\phi$

$$\dot{\mathbf{X}}' = F_X + G_X \mathbf{u}_X + \Delta_{\mathbf{X}'}, \mathbf{u}_X = \begin{bmatrix} \alpha & \beta \end{bmatrix}^T, \Delta_{\mathbf{X}'} = [\Delta f_x \quad \Delta f_y]^T$$
$$F_X = \begin{bmatrix} \cos\theta\cos\psi(qw - rv) \\ \cos\phi\cos\psi(ru - pw) \end{bmatrix}, G_X = \frac{U}{m} \begin{bmatrix} \sin\psi & \cos\psi \\ -\cos\psi & \sin\psi \end{bmatrix} \tag{15}$$

where $\mathbf{X}' = (\dot{x}, \dot{y})$, G_X is nonsingular when $U > 0$. As the relative degree $r_x + r_y = 2 + 2 = 4$, zero dynamic does not exist. The DI position control law is designed as

$$\begin{aligned} \mathbf{u}_X &= G_X^{-1}(\mathbf{v}_{\mathbf{X}} - F_X - \Delta_{\mathbf{X}'}), \mathbf{v}_{\mathbf{X}} = (v_x, v_y)^T \\ v_x &= \ddot{x}_d - k_{x1}(\dot{x} - \dot{x}_d) - k_{x2}(x - x_d) \\ v_y &= \ddot{y}_d - k_{y1}(\dot{y} - \dot{y}_d) - k_{y2}(y - y_d) \end{aligned} \tag{16}$$

when $k_{x1}, k_{x2}, k_{y1}, k_{y2} > 0$, the error equations are Hurwitz and exponentially stable. Since $-\pi/2 < \phi, \theta < \pi/2$, there is $-1 < \alpha < 1, -\sqrt{1-\alpha^2} < \beta < \sqrt{1-\alpha^2}$, and the desired angles θ_d, ϕ_d can be given as follows.

$$\phi_d = \arcsin(\alpha), \ \theta_d = \arcsin(\beta / \sqrt{1-\alpha^2}) \tag{17}$$

Similarly, consider the angle loop subsystem

$$\dot{\boldsymbol{\xi}} = G_\xi \boldsymbol{\Omega}, G_\xi = \begin{bmatrix} 0 & \sin\phi\sec\theta & \cos\phi\sec\theta \\ 0 & \cos\phi & -\sin\phi \\ 1 & \sin\phi\tan\theta & \cos\phi\tan\theta \end{bmatrix} \tag{18}$$

$r_\phi + r_\theta + r_\psi = 1 + 1 + 1 = 3$, so the relative degree equals the degree of the system. As no zero dynamic exists, the control law can be designed as follow to provide the desired angular rate $\boldsymbol{\Omega}_d = \mathbf{u}_\xi = (p_d, q_d, r_d)$.

$$\mathbf{u}_\xi = G_\xi^{-1}\mathbf{v}_\xi, \begin{aligned} v_\phi &= \dot{\phi}_d - k_\phi(\phi - \phi_d), \\ v_\theta &= \theta_d - k_\theta(\theta - \theta_d), \\ v_\phi &= \dot{\psi}_d - k_\psi(\psi - \psi_d) \end{aligned} \quad \Bigg\| \quad k_\phi, k_\theta, k_\psi > 0 \tag{19}$$

$G_\xi = -\sec\theta$, so it is nonsingular when $\theta < \pi/2$. The error equations of angle is Hurwitz when parameters satisfy the requirements in (19), thus the DI control law for the angle loop can guarantee the errors exponentially stable.

B. The inner-loop controller based on Incremental Nonlinear Dynamic Inverse (INDI)

The inner loop combines angular rate control and altitude control together. Denoting $\boldsymbol{\lambda} = (p, q, r, \dot{z})^T$, the nonlinear form based on (6), (11) can be written as

$$\dot{\boldsymbol{\lambda}} = F(p,q,r) + H_1(p,q)\mathbf{w} + H_2\dot{\mathbf{w}} + H_3 diag(\mathbf{w})\mathbf{w} + \boldsymbol{\Delta}_{\mathbf{disturb}} \quad (20)$$

$$F(p,q,r) = \begin{bmatrix} (I_y - I_z)qr / I_x \\ (I_z - I_x)pr / I_y \\ (I_x - I_y)pq / I_z \\ -g \end{bmatrix}, H_2 = \begin{bmatrix} 0 & 0 & 0 & 0 \\ 0 & 0 & 0 & 0 \\ J_r / I_z & J_r / I_z & J_r / I_z & J_r / I_z \\ 0 & 0 & 0 & 0 \end{bmatrix}$$

$$H_1 = \begin{bmatrix} -J_r q / I_x & J_r q / I_x & -J_r q / I_x & J_r q / I_x \\ J_r p / I_y & -J_r p / I_y & J_r p / I_y & -J_r p / I_y \\ 0 & 0 & 0 & 0 \\ 0 & 0 & 0 & 0 \end{bmatrix}$$

$$H_3 = \begin{bmatrix} 0 & -lk_T / I_x & 0 & lk_T / I_x \\ lk_T / I_y & 0 & -lk_T / I_y & 0 \\ k_d / I_z & -k_d / I_z & k_d / I_z & -k_d / I_z \\ \frac{k_T c\theta c\phi}{m} & \frac{k_T c\theta c\phi}{m} & \frac{k_T c\theta c\phi}{m} & \frac{k_T c\theta c\phi}{m} \end{bmatrix} \quad (21)$$

The inner loop nonlinear form $\dot{\mathbf{x}} = f(\mathbf{x}) + g(\mathbf{x}, \dot{u}, u^T u, u)$ is not affine, thus requirements of DI control cannot be satisfied. The incremental nonlinear dynamic inversion (INDI) is developed in our control scheme to solve it. Denoting the states of last sample time as $S_0 = (\phi_0, \theta_0, p_0, q_0, r_0, z_0, \mathbf{w_0})$, we do first-order Tylor expansion around S_0.

$$\begin{aligned} F(p,q,r) &= F(p_0,q_0,r_0) + \frac{\delta F}{\delta p}\Delta p + \frac{\delta F}{\delta q}\Delta q + \frac{\delta F}{\delta r}\Delta r \\ H_1(p,q)\mathbf{w} &= (H_1(p_0,q_0) + \frac{\delta H_1}{\delta p}\Delta p + \frac{\delta H_1}{\delta q}\Delta q)\mathbf{w_0} \\ &\quad + H_1(p_0,q_0)(\mathbf{w} - \mathbf{w_0}) \\ H_2\dot{\mathbf{w}} &= H_2\dot{\mathbf{w}}_{\mathbf{0}} + H_2\ddot{\mathbf{w}}_{\mathbf{0}}(\dot{\mathbf{w}} - \dot{\mathbf{w}}_{\mathbf{0}}) \\ H_3 diag(\mathbf{w})\mathbf{w} &= H_3 diag(\mathbf{w_0})\mathbf{w_0} + 2H_3 diag(\mathbf{w_0})(\mathbf{w} - \mathbf{w_0}) \end{aligned} \quad (22)$$

$$\begin{aligned} \dot{\boldsymbol{\lambda}}_{\mathbf{0}} &= F(p_0,q_0,r_0) + H_1(p_0,q_0)\mathbf{w_0} + H_2\dot{\mathbf{w}}_{\mathbf{0}} \\ &\quad + H_3(z_0) diag(\mathbf{w_0})\mathbf{w_0} \end{aligned} \quad (23)$$

The second order derivative term in third equation of (22) is regarded as part of disturbance $\boldsymbol{\Delta}_{\mathbf{disturb}}$. Then (20) can be rewritten as

$$\dot{\boldsymbol{\lambda}} = \dot{\boldsymbol{\lambda}}_{\mathbf{0}} + \mathbf{F}' + \mathbf{G}'(\mathbf{w} - \mathbf{w_0}) + \boldsymbol{\Delta}_{\mathbf{disturb}} \quad (24)$$

in which $\mathbf{F}'$ and $\mathbf{G}'$ can be formulated as

$$\begin{aligned} \mathbf{F}' &= \frac{\delta F}{\delta p}\Delta p + \frac{\delta F}{\delta q}\Delta q + \frac{\delta F}{\delta r}\Delta r + (\frac{\delta H_1}{\delta p}\Delta p + \frac{\delta H_1}{\delta q}\Delta q)\mathbf{w_0}, \\ &= \begin{bmatrix} (I_y - I_z)/I_x(\Delta q r_0 + \Delta r q_0) + J_r \Delta q / I_x(-w_{01} + w_{02} - w_{03} + w_{04}) \\ (I_z - I_x)/I_y(\Delta p r_0 + \Delta r p_0) + J_r \Delta p / I_y(w_{01} - w_{02} + w_{03} - w_{04}) \\ (I_x - I_y)/I_z(\Delta p q_0 + \Delta q p_0) \\ 0 \end{bmatrix} \end{aligned} \quad (25)$$

in which $\mathbf{w_0}$ expresses the velocities of the four rotors in last sample time. Denote $\mathbf{w_0} = (w_{01}, w_{02}, w_{03}, w_{04})^T$.

$$\mathbf{G}' = H_1(p_0, q_0) + 2H_3 diag(\mathbf{w_0}) \quad (26)$$

It is obvious that the relative degrees $r_p + r_q + r_r + r_z = 5$, which equals the system degree, so there is no zero dynamics. The disturbance $\boldsymbol{\Delta}_{\mathbf{disturb}}$ is observed and compensated by IESO, which will be described in Section IV. $\mathbf{G}'$ can be verified nonsingular, then the control law is designed as

$$\mathbf{u} = \mathbf{w_0} + \mathbf{G}'^{-1}(\mathbf{v} - \mathbf{F}' - \dot{\boldsymbol{\lambda}}_{\mathbf{0}} - \boldsymbol{\Delta}_{\mathbf{disturb}}) \quad (27)$$

Taking (27) into (24), we get $\dot{\boldsymbol{\lambda}} = \mathbf{v}$. Denoting $(\boldsymbol{\Omega}_{\mathbf{d}}(p_d, q_d, r_d), z_d)$ as the desired angular rate, the virtual control is designed as

$$\begin{aligned} &v_1 = \dot{p}_d - \lambda_p e_p, v_2 = \dot{q}_d - \lambda_q e_q, v_3 = \dot{r}_d - \lambda_r e_r, \\ &v_4 = \ddot{z}_d - \lambda_{z1}\dot{e}_z - \lambda_{z2} e_z \\ &\lambda_p, \lambda_q, \lambda_r, \lambda_{z1}, \lambda_{z2} > 0 \end{aligned} \quad (28)$$

Denoting $\mathbf{e}_{\boldsymbol{\Omega}} = \boldsymbol{\Omega} - \boldsymbol{\Omega}_{\mathbf{d}}, e_z = z - z_d$, the error equations can be written as

$$\dot{\mathbf{e}}_{\boldsymbol{\Omega}} + K_1 \mathbf{e}_{\boldsymbol{\Omega}} = 0 \ , \ \ddot{e}_z + K_{21}\dot{e}_z + K_{22} e_z = 0 \quad (29)$$

when $K_1 > 0$, $K_{21}, K_{22} > 0$, the equations in (30) are both Hurwitz. As a result, e_p, e_q, e_r, e_z realize exponentially stable.

IV. Design of Integral Extended State Observer and Arranged Transient Process

The uncertainties and external disturbance $\Delta_{\mathbf{X}'}$, $\boldsymbol{\Delta}_{\mathbf{disturb}}$ in (14) and (20) are concerned in the control scheme design in Section III. The disturbances can not be eliminated by the INDI or DI controller itself. IESO is adopted in our control scheme to estimate the disturbance and make the compensation. The ground effect can be observed as part of "disturbance" and compensated at the same time. The integral extended state observer has the advantage over classical ESO in attenuating the measurement noises.

A. Design of Integral Extend State Observer (IESO)

Due to the length limitation, we just take the IESO design of the altitude for example. The measured altitude poisoned by noise is denoted as $\tilde{z} = z + n(t)$. The integration of which is denoted as $z_0 = \int \tilde{z} dt$. Altitude subsystem can be rewritten as

$$
\begin{aligned}
\dot{z}_0 &= \tilde{z} = z_1 + n(t) \\
\dot{z}_1 &= z_2 \\
\dot{z}_2 &= \frac{1}{m}(\cos\theta\cos\phi k_T \mathbf{w}^T\mathbf{w}) + f_{col}^z + \Delta f_z' \\
\Delta f_z' &= \Delta f_z + (\cos\theta\cos\phi k_T \mathbf{w}^T\mathbf{w})(G_{ef}(z)-1)/m
\end{aligned} \tag{30}
$$

in which f_{col}^z is the z component of Coriolis force in (6). The IESO for altitude is designed to observe $\Delta f_z'$, which includes disturbances and the component of ground effect. The IESO of altitude can be written as

$$
\begin{aligned}
e &= x_0 - z_0 \\
\dot{x}_0 &= x_1 - \beta_1 e \\
\dot{x}_1 &= x_2 - \beta_2 fal(e,\alpha_1,\delta) \\
\dot{x}_2 &= x_3 - \beta_3 fal(e,\alpha_2,\delta) + \frac{1}{m}(\cos\theta\cos\phi k_T \mathbf{w}^T\mathbf{w}) + f_{col}^z \\
\dot{x}_3 &= -\beta_4 fal(e,\alpha_3,\delta)
\end{aligned} \tag{31}
$$

where $x_0 \to z_0, x_1 \to z_1, x_2 \to z_2, x_3 \to \Delta f_z'$. The definition of function $fal(e,\alpha,\delta)$ can be found in [11]. The disturbance is estimated by extended state x_3 . For an n-order system, IESO has n+2 orders. The IESO design of other states is similar to that of the altitude.

B. Design of Arranged Transient Process (ATP)

ATP is developed in our control scheme to solve the problem that the desired input generated by another control loop jumps so huge that the subsequent loop cannot keep pace. Tracking differentiator (TD) is adopted in our control scheme to work as arrange transient process, which is proposed by Han in ADRC [11]. Limited by the length of the paper, the altitude is taken as example to describe the TD

$$
\begin{aligned}
x_1(k+1) &= x_1(k) + hx_2(k) \\
x_2(k+1) &= x_2(k) + hfst(x_1(k) - z_d, x_2(k), r, h_0)
\end{aligned} \tag{32}
$$

where h is the sample period. $x_1(k)$ and $x_2(k)$ are states of arranged process and their derivative. z_d is the original reference altitude. The definition of fst can be found in [11]. r and h_0 are called "speed factor" and "filter factor" respectively, which decide the tracking performance.

V. SIMULATION

Three contrast simulations are designed as follows. Firstly, a contrast simulation is designed to prove the effectiveness of IESO in improving the taking off performance when influenced by ground effect. Secondly, the gusty wind influences are concerned in system. The simulation validates the disturbance rejection effectiveness of the control scheme. Finally, the 20% uniform white noises are concerned for angular rate measurement to validate the effectiveness of the control scheme in noise attenuation. The initial states are $\mathbf{X} = \mathbf{V} = \boldsymbol{\xi} = \boldsymbol{\Omega} = \mathbf{0}$. The reference states are $x_d = 1, y_d = 2$, $z_d = 2$. $\psi_d = 10\pi/180(rad)$. The model variables and the parameters of control scheme are listed in Table I.

A contrast simulation is conducted to compare the tracking performance in altitude under two circumstances: 1) With IESO, 2) Without IESO.

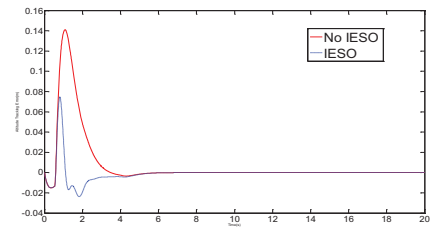

Figure 2. Tracking errors in altitude with IESO or without IESO

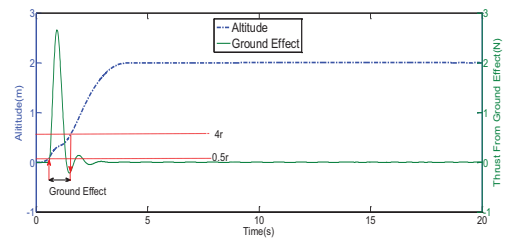

Figure 3. Ground effect observation by IESO

From the results depicted in Figure 2, the IESO is important in decreasing the tracking error brought by ground effect. The additional thrust provided by ground effect is estimated by IESO in Figure 3. Furthermore, the observed ground effect function in Figure 3 region corresponds to the function region in (12).

The second contrast simulation is conducted to prove the disturbance rejection performance of our control scheme. Assume that $\Delta_{\mathbf{X}'} = (0.1\text{sign}(\sin(t)), -0.1\text{sign}(\sin(t)))^T$, and $\boldsymbol{\Delta}_{\mathbf{disturb}} = (0,0,0,0.5sign(\sin(t)))$, in which $\Delta_{\mathbf{X}'}$ and $\boldsymbol{\Delta}_{\mathbf{disturb}}$ are the external disturbances in (14) and (20). The control with IESO and the control without ESO are compared in Figure 4.

Figure 4 shows the disturbance rejection performance in the trajectory tracking control under two circumstances:1) Group 1,without IESO; 2) Group2, with IESO. It can be concluded that both group 1 and 2 realize the good tracking control effect. However, the group 2 with IESO gains better performance in disturbance rejection.

The last contrast simulation is conducted to validate the robustness of the scheme against measurement noise. The Group 1 and 2 share the same complete control scheme, as well as the same external disturbance as simulation above. While the The only difference is, there is no measurement noise in group 1 and angular rates in Group 2 are poisoned by 20% measurement uniform white noise.

From Figure 5, it can be concluded that Group 1 and 2 share the similar performance in both trajectory tracking and yaw tracking performances, and both perform well in tracking control. Obviously, the robustness against measurement noise of our control scheme is validated.

TABLE I. MODEL VARIABLES AND PARAMETERS OF CONTROL SCHEME

Quadrotor Model Variables	*ATP*	*Inner IESO*	*Outer IESO*	*DI*	*INDI*
$k_T = 5.5\times10^{-5}, k_d = 1.1\times10^{-6}(m\cdot s^{-2})$	$r_{xy} = 0.1, r_z = 0.5$	$\beta_1 = 100, \beta_2 = 300$	$\beta_1 = 150, \beta_2 = 500$	$k_\phi = k_\theta = 2$	$k_p = k_q = 20$
$J_x = J_y = 8\times10^{-3}, J_z = 1.4\times10^{-2}(kg\cdot m^2)$	$r_\xi = 1,\ r_\Omega = 2$	$\beta_3 = 1000, \beta_4 = 3000$	$\beta_3 = 1500, \beta_4 = 4000$	$k_\psi = 0.7$	$k_r = 10$
$J_r = 1.0\times10^{-4}(kg\cdot m^2)$ $, m = 1kg, l = 0.24m$	$h = 0.01, h_0 = 0.05$	$\alpha_1 = 0.5, \alpha_2 = 0.25$		$k_{x1} = k_{y1} = 3$	$k_{z1} = 6.25, k_{z2} = 5$
$r = 0.12m,\ z_{cg} = 0.05m,\ \eta = 8$		$\alpha_3 = 0.125, \delta = 0.5$		$k_{x2} = k_{y2} = 1.5$	

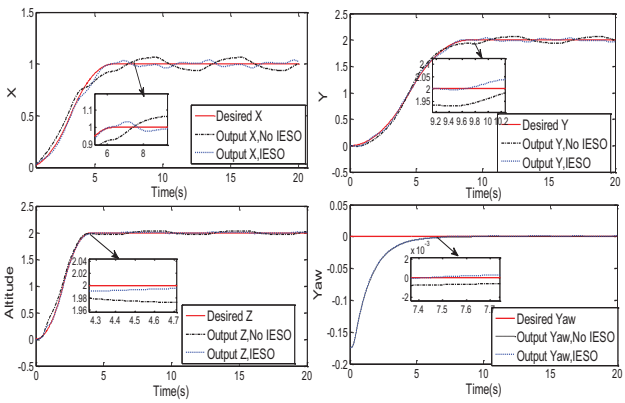

Figure 4. Disturbance rejection performances in tracking control

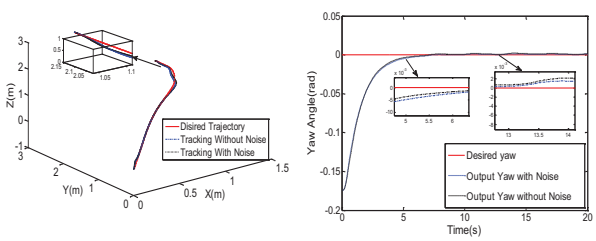

Figure 5. Measurement noise attenuation performance

VI. CONCLUSION

In this paper, an advanced control scheme is proposed for trajectory tracking control of quadrotor during taking off process. Firstly, the high-fidelity model is established for the quadrotor with Coriolis force, gyro effect and the ground effect taken into account. Then the quadrotor system is decoupled into three fully-actuated control loops as time-scale separation principle. Moreover, a new incremental nonlinear dynamic inversion (INDI) control law is developed to solve the non-affine form of inner loop. The angle loop and position loop are controlled with dynamic inverse (DI) control laws. The DI and INDI control laws in the scheme are confirmed exponentially stable when their error equations are guaranteed Hurwitz. To compensate the external disturbance and attenuate the measurement noise, the integrated extended state observer (IESO) is incorporated into the control scheme. The arranged transient process (ATP) makes great difference in smoothing and filtering huge-jumped desired value. Finally, the contrast simulations prove the ability of IESO to observe and compensate the influence brought by ground effect. Furthermore, the effectiveness of control scheme in trajectory tracking control, disturbance rejection, and measurement noise attenuation are validated.

REFERENCES

[1] Y. Zhang, W. Zhao, L. U. Tiansheng, and L. I. Jingsong, "The attitude control of the four-rotor unmanned helicopter based on feedback linearization control," *Wseas Transaction on Systems*. vol. 14, no.3, pp.129, 2013.

[2] I. C. Cheeseman and W. E. Bennett, "The effect of ground on a helicopter rotor in forward flight," in *Aeronautical Research Council*, 1957.

[3] G. Hoffmann, "Quadrotor Helicopter Trajectory Tracking Control," in *Guidance, Navigation, and Control Conf*, *AIAA 2008-7410*, 2008.

[4] H. Jafari, M. Zareh, J. Roshanian, and A. Nikkhah, "An Optimal Guidance Law Applied to Quadrotor Using LQR Method," *Transactions of the Japan Society for Aeronautical & Space Sciences*, vol. 53, no.2, pp. 32-39, 2010.

[5] S. Bouabdallah and R. Siegwart, "Backstepping and Sliding-mode Techniques Applied to an Indoor Micro Quadrotor," in *Proc of the 2005 IEEE International Conference on Robotics and Automation*, April 18-22, 2005, Barcelona, Spain, 2005, pp. 2247-2252.

[6] M. A. M. Basri, A. R. Husain, and K. A. Danapalasingam, "Enhanced Backstepping Controller Design with Application to Autonomous Quadrotor Unmanned Aerial Vehicle," *Journal of Intelligent & Robotic Systems*, vol. 79, no.5 , pp. 295-321, 2015.

[7] J. S. Li and X. Cao, "Attitude control of small unmanned four-rotor helicopter based on adaptive inverse control theory," *Mechanika*, vol. 18, no.1, pp. 89-93, 2012.

[8] H. Voos, "Nonlinear and neural network-based control of a small four-rotor aerial robot," *IEEE/ASME international conference on Advanced intelligent mechatronics*, 2007, pp. 1-6.

[9] E. J. J. Smeur, Q. Chu, and G. C. H. E. D. Croon, "Adaptive Incremental Nonlinear Dynamic Inversion for Attitude Control of Micro Air Vehicles," *Journal of Guidance Control & Dynamics*, pp. 1-12, 2015.

[10] A. Benallegue, A. Mokhtari, and L. Fridman, "High order sliding mode observer for a quadrotor UAV," *International Journal of Robust & Nonlinear Control*, vol. 18, pp. 427-440, 2008.

[11] J. Han, "From PID to Active Disturbance Rejection Control," *IEEE Transactions on Industrial Electronics*, vol. 56, 2009.

[12] G. Zuoxin, "The stability and filtering performance of extend state observer (Post Doctor Report, in chinese)," pp.42-50, 2002.

[13] L. Danjun, Z. Yan, S. Zongying, and L. Geng, "Autonomous landing of quadrotor based on ground effect modelling," *in 34th Chinese Control Conference (CCC)*, 2015.